

# Simulating the Kinetics and Thermodynamics of Transitions via Forward Flux/Umbrella Sampling

Ernesto E. Borrero and Fernando A. Escobedo\*

School of Chemical and Biomolecular Engineering, Cornell University, Ithaca, New York 14853

Received: October 14, 2008; Revised Manuscript Received: March 13, 2009

First, a technique is introduced for computing equilibrium probability distributions for transitional rare-event simulations by combining the ensemble of trajectories generated by forward flux sampling (FFS) and by umbrella sampling (US) in multiple windows along an order parameter of interest; this method is denoted FFS-US. Second, the FFS algorithm is extended to obtain rate constants of partial transitions involving intermediate states from a single simulation; this is denoted “multiple state” FFS. For the FFS-US method, a FFS algorithm (preoptimized for order parameter and staging) is used to take advantage of its zero potential bias of phase-space sampling to gather histogram data with which to jump start the US and get the equilibrium distributions. In this way, kinetic data (like the rate constants and the transition path ensemble) and the underlying free-energy landscape (or probability distribution) of the system are obtained efficiently and concurrently. The applicability of these techniques is illustrated by studying several test systems, including two that involve potential energy surfaces having multiple metastable states and transition pathways, representative of complex kinetic behavior.

## I. Introduction

Many processes in complex molecular systems involve rare events, e.g., in phase transitions and conformational changes between stable or metastable states. Simulating the transition kinetics (i.e., rate constants and mechanistic details) and the relative free energies of such metastable basins and those associated with intervening barriers are thus central objectives in many applications of computational physical chemistry. However, conventional numerical techniques are impractical for the simultaneous computation of free energies and kinetics of rare events. Schemes such as forward flux sampling<sup>1,2</sup> (FFS) allow the computation of rate constants by overcoming the problem associated with simulating rare events (i.e., enhancing the sampling by a series of interfaces that partition the phase space and reducing the CPU time wasted on the uneventful waiting time between events), while techniques such as umbrella sampling<sup>3</sup> (US) allow the calculation of free energy barriers separating the stable states. In this article, we explored the idea of using the framework of FFS to evaluate both the kinetics of the transition pathways and the underlying free energy landscape. The proposed approach, to be denoted FFS-US, computes free energies using the ensemble of trajectories generated by a FFS scheme combined with US data for windows defined by the FFS interfaces. Essentially, FFS-US combines the zero-potential-bias data from FFS with additional US data to calculate the potential of mean force along a chosen reaction coordinate (i.e., order parameter).

Other research groups have proposed schemes for the simultaneous computation of free energies and kinetics of rare events. For example, Radhakrishnan and Schlick<sup>4</sup> developed “BOLAS”, a scheme for free energy calculations, by combining the Monte Carlo (MC) ensemble of trajectories from the shooting algorithm of transition path sampling (TPS) with the window-based US strategy to enhance the efficiency of comput-

ing the probability density distribution  $p(\lambda)$  (i.e., the probability to find the system at a certain value of the order parameter  $\lambda$ ) over a desired range of the reaction coordinate. Moroni et al.<sup>5</sup> also introduced a method to evaluate simultaneously the transition rate constant and the free energy profile using partial path transition interface sampling (PPTIS) scheme. Their method corrects the bias introduced in the path ensemble obtained by the PPTIS formalism by comparing neighboring interface ensembles. For this purpose, suitable weights are calculated for the histograms of points visited around the outer interfaces for two consecutive windows and used to scale the ensembles of states visited around the inner interface. The resulting histograms of the probability density  $p(\lambda)$  on each window are matched together to obtain the continuous  $p(\lambda)$  distribution. The milestone method proposed by Faradjian and Elber<sup>6</sup> also employs a series of interfaces to estimate the average transition rate constant and  $p(\lambda)$ , assuming that the partial transitions between consecutive interfaces do not depend upon the full history of the path. Both PPTIS and milestones are applicable to systems in thermodynamic equilibrium. Ytreberg and Zuckerman<sup>7</sup> developed the “black-box” strategy for reweighting any ensemble of arbitrarily generated configurations to produce a canonically distributed ensemble and estimate free energy differences.

Recently, Valeriani et al.<sup>8</sup> introduced a method for computing stationary distributions (i.e., the “free energy” profile and the steady-state probability distribution for equilibrium and non-equilibrium systems, respectively) using FFS schemes. In their method, the stationary distribution  $P_{ss}(\lambda) = P(\lambda)$  along a reaction coordinate  $\lambda$  is obtained by performing two FFS simulations to obtain the rate constants for the forward and backward transitions. These rates are then used to reweigh contributions to  $P(\lambda)$  from trajectories originating from both region A and region B. The need of performing these two FFS simulations can be a shortcoming of this method because in many applications only one transition is of interest (e.g., the folding of a protein as opposed to unfolding) and if one state is much more stable than

\* To whom correspondence should be addressed. E-mail: fe13@cornell.edu.

the other, then sampling the transition toward the less stable state may be computationally very demanding. A related method to estimate  $P(\lambda)$  has also been proposed<sup>9</sup> by matching histograms from backward and forward reactions in transition interface sampling (TIS) simulations.

The proposed FFS-US method can be seen as complementary to that of Valeriani et al.<sup>8</sup> wherein rather than performing an additional FFS simulation (for the reverse transition), the US strategy is implemented following an original FFS protocol. Once the FFS run has ended, the transition path ensemble is reweighted (following a scheme akin to that of Moroni et al.<sup>5</sup>) and the US takes over to sample the regions inside the corresponding windows  $w_i$  (bounded by the hard walls at interfaces  $\lambda_i$  and  $\lambda_{i+1}$ ) until the partial path ensemble loses any “memory” of where it originated. However, the FFS-US method is more limited than Valeriani et al.’s method in that the former is only indicated for equilibrium probability distributions. Wamflash et al.<sup>10</sup> has presented an algorithm that can also determine the steady-state probability distribution for nonequilibrium processes by transferring information about fluxes and probabilities between neighboring US regions (to correct for the lack of detailed balance). While a FFS approach could potentially be designed to extract such information (and thus generalize the uses of FFS-US), this lies beyond the scope of this work.

A second goal of this paper is to extend the original FFS formalism to study transitions that involve intermediate states by using concepts similar to those of the multiple state transition path sampling method by Rogal and Bolhuis.<sup>13</sup> In the multiple state FFS method, the rate constant estimates for all forward reactions including transitions that go from basin A to B through intermediate states and from A to any intermediate state are calculated from one single simulation rather than from separate FFS simulations for each partial reaction.

This paper complements two previous articles in which we addressed several challenges of applying a FFS-type algorithm for the simulation of complex system; namely: (i) a method to determine an adequate reaction coordinate (i.e., order parameter) to describe the system’s dynamics (denoted FFS-LSE)<sup>11</sup> and (ii) an adaptive algorithm to optimize for either the number and position of the interfaces (i.e., optimized  $\lambda$  phase staging), and/or the number of fired trial runs per interface<sup>12</sup> to reduce the statistical error in the rate constant estimation (for a given computational cost). Our strategy here is thus to take full advantage of this platform—the optimized order parameter, staging, and collection of transition paths obtained from a FFS simulation—to set up a complementary US run to obtain free-energy information.

By way of background, we start by briefly reviewing the FFS-type simulation scheme for the calculation of rate constants and transition pathways (section II A) and the US protocol (subsection II B). In sections II C and II D, we discuss how the US was implemented within the FFS framework to map the energy landscape. In section II E, we introduce the formalism for multiple state FFS simulations. In section III, we apply the FFS-US approach to several test cases including two-dimensional rugged energy surfaces that are representative of numerous complex systems. We also compare in this section the thermodynamic results for the test systems with those from straight brute-force calculations. In section IV, we provide some concluding remarks.

## II. Methods

**A. Forward Flux Sampling (FFS).** In this work, we focus the discussion on two of the three path sampling schemes

proposed in the literature to generate transition paths by a FFS-type approach: (i) the direct forward flux sampling (DFFS), and (ii) the branched growth method (BG).<sup>1,2</sup> Essentially, these schemes sample the transition path ensemble (TPE) by performing MC sampling of dynamic trajectories between interfaces. The rate constant of the process is estimated as an average rate of transitions from two well-defined states A and B using an “effective positive flux” expression.<sup>1,2,14,15</sup> An order parameter  $\lambda(x)$  (where  $x$  is the phase space coordinates) is used to partition the phase space by employing a series of nonintersecting interfaces ( $n + 1$ ) such that the system is considered in region A for  $\lambda(x) \leq \lambda_A(x)$  and in region B for  $\lambda(x) \geq \lambda_B(x)$ . The effective flux expression estimates the rate constant  $k_{A \rightarrow B}$  for transitions from A to B as<sup>1,2</sup>

$$k_{A \rightarrow B} = \bar{\Phi}_{A,0} P(\lambda_{n=B} | \lambda_0) \quad (1)$$

where  $\bar{\Phi}_{A,0}$  is the total average flux of trajectories from A to  $\lambda_0$ , and  $P(\lambda_{n=B} | \lambda_0)$  is the probability that a trajectory reaching  $\lambda_0$  from A will reach to B without returning to A.<sup>1</sup> Likewise,  $P(\lambda_{n=B} | \lambda_0)$  can be expressed as the product of conditional probabilities:

$$P(\lambda_{n=B} | \lambda_0) = \prod_{i=0}^{n-1} P(\lambda_{i+1} | \lambda_i) \quad (2)$$

where  $P(\lambda_{i+1} | \lambda_i)$  is the probability that a trajectory that visits A and crosses  $\lambda_i$  for the first time will subsequently reach  $\lambda_{i+1}$  without returning to the initial region A.<sup>12</sup> For a complete description of the theoretical background of the algorithm, see ref 1.

**B. Umbrella Sampling (US).** The potential of mean force  $F_i(\lambda)$  is calculated by measuring the probability distribution  $p_i(\lambda)$  to be at a certain value of the order parameter  $\lambda$  chosen a priori to describe the transition between basins A and B:

$$F_i(\lambda) = -k_B T \ln[p_i(\lambda)] + \text{const} \quad (3)$$

To enhance the efficiency of computing  $p_i(\lambda)$  over the desired range of  $\lambda$ , we essentially performed a window-based US strategy. The desired range in the phase space is divided up in smaller windows,  $w_i$  ( $\lambda_0 \leq \lambda_i \leq \lambda_{i+1}$ ), and the walls are used as hard boundaries [i.e., states are accepted only if they visit the region inside the window]. This is equivalent to performing an US with a weighting function of zero inside the window. The functions  $F_i(\lambda)$  in different windows are pieced together by matching the constants such that the entire function  $F(\lambda)$  is continuous at the boundaries of the windows. Hence, after a predetermined number of statistics per window are accumulated, the un-normalized  $p(\lambda)$  distribution can be estimated recursively<sup>16</sup>

$$\frac{p(\lambda)}{p(0)} = \frac{H_{0r} H_{1r}}{H_{0l} H_{1l}} \cdots \frac{H_i(\lambda)}{H_{il}} = \prod_{n=1}^{i-1} r_i \frac{H_i(\lambda)}{H_{il}} \quad (4)$$

where  $\lambda \in [\lambda_i, \lambda_{i+1}]$ . A histogram  $H_i(\lambda)$  monitors how often each state is visited in the  $i$ th window  $[\lambda_i, \lambda_{i+1}]$ , where  $\lambda_i$  is the interface in which trial runs are initiated in the FFS method. The log of ratios  $r_i = H_{ir}/H_{il}$  in eq 4 correspond to free energy differences, and  $H_{il} \equiv H_i(\lambda_{i-1})$  and  $H_{ir} \equiv H_i(\lambda_{i+1})$  denote the values of the  $i$ th histogram at its left and right boundary, respectively. When evaluating  $H_i(\lambda)$ , if a move attempts to leave the  $w_i$ , it will be rejected and  $H$  [at the window edge] incremented by one to fulfill detailed balance.<sup>8,16</sup> However, if the location of a window (in the free-energy space) is such that a strong force drives the system toward the front or back wall, the method could lead to artificial spikes in probability density at a window edge. To avoid this, one could increment the

nominal window's size a little to  $[\lambda_i - \Delta\lambda, \lambda_{i+1} + \Delta\lambda]$ , and only count statistics inside the  $[\lambda_i, \lambda_{i+1}]$  region for the  $H_i(\lambda)$  histogram.

**C.  $N_{\text{bin}}$  and  $N_{\text{win}}^{(i)}$ .** The overall error in  $p_i(\lambda)$  depends on the choice of the number of statistics accumulated per window  $i$  ( $N_{\text{win}}^{(i)}$ ) and the minimum number of entries per bin ( $N_{\text{bin}}$ ).  $N_{\text{win}}^{(i)}$  is essentially the time  $t_{w_i}$  (in units in number of steps) needed to obtain a predetermined relative statistical error in  $p_i(\lambda)$ , estimated to be

$$N_{\text{win}}^{(i)} \approx t_{w_i} = a\omega_i^2 \quad (5)$$

where  $\omega_i$  is the window size and  $a$  is a proportionality constant.<sup>16</sup> If all the windows are the same size  $\omega_i = \omega$ , the total computational time to sample the complete phase space is

$$t_{\text{CPU}} = \sum_{i=1}^m t_{\omega_i} = a \sum_{i=1}^m \omega_i^2 = am\omega^2 \quad (6)$$

where  $m$  denotes the number of windows into which the phase space was subdivided. In the limit of a single large window (i.e.,  $m = 1$  and  $\omega' = m\omega$ ), the total computational time for a standard brute force (BF) simulation is

$$t'_{\text{CPU}} = a\omega'^2 = a(m\omega)^2 = mt_{\text{CPU}} \quad (7)$$

Showing the known fact that the basic window strategy reduces the computational effort by a factor of  $m$ .<sup>3,16</sup> Hence, for a fixed number of windows and an estimated  $t'_{\text{CPU}}$  value,  $N_{\text{win}}^{(i)}$  is calculated from eq 5, where the constant  $a$  is estimated using eqs 6 and 7. Sampling inside the window's region,  $w_i$ , should therefore be continued until satisfying the condition

$$\sum_{\lambda=\lambda_i}^{\lambda_{i+1}} H_i(\lambda) \geq N_{\text{win}}^{(i)} \quad (8)$$

While  $N_{\text{win}}^{(i)}$  sets a bound on the number of statistics needed for each histogram in window  $w_i$ ,  $N_{\text{bin}}$  sets a limit for the minimum amount of local sampling (in a given bin). To estimate  $N_{\text{bin}}$ , we assume that the number of points per bin follows a Poisson distribution and therefore the relative statistical error ( $\delta$ ) in  $p_i(\lambda)$  is given by<sup>17</sup>

$$\delta \propto [N_{\text{bin}}]^{-1/2} \quad (9)$$

from which it is clear that  $\delta$  always decreases as additional statistics are added to the histogram  $H_i(\lambda)$  in the  $w_i$ . Thus, for any one  $l$  bin,  $N_{\text{bin}}$  should be in the range  $[10^2, 10^4]$  in order to obtain a  $\delta$  of order  $\Delta_l \sim O(10^{-2})$ . Based on this, we assumed that at each interface "memory effects" may persist for longer than the time needed to travel from one interface to the other (i.e., from  $\lambda_i$  to  $\lambda_{i-1}$  or  $\lambda_{i+1}$ ), but not much longer than the time required to satisfy the condition

$$\min[H_i(\lambda)] \geq N_{\text{bin}} \quad (10)$$

i.e., this condition implies that the overall error  $\Delta$  for  $H_i(\lambda)$  is of order  $\Delta \sim O(\Delta_l)$ .

In summary, the correct probability distribution in the  $i$ th window is obtained by accumulating statistics in  $H_i(\lambda)$  until the conditions in eqs 8 and 10 are met. In section III, we discuss how the values for  $N_{\text{win}}^{(i)}$  and  $N_{\text{bin}}$  correlate to the statistical error in  $p_i(\lambda)$ .

**D. FFS-US Combination.** In this section, we introduce the proposed method, FFS-US, for efficient calculation of probability distributions following the simulation of the rate transition constant and the transition state ensemble (TPE). The FFS-type formalism generates partial paths between interfaces by initiating

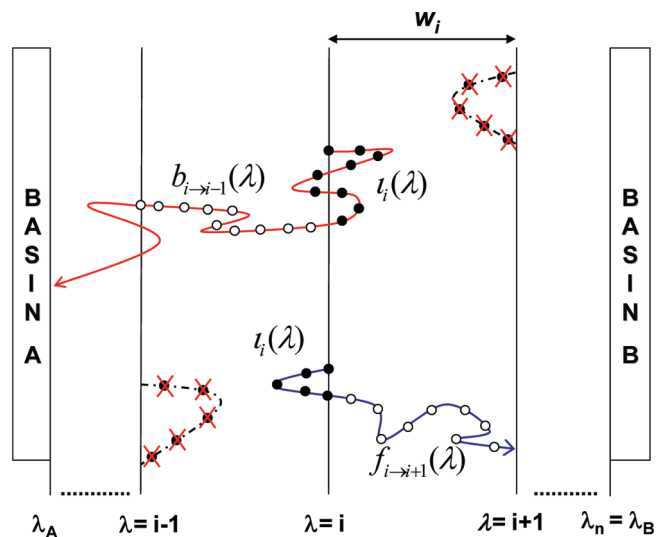


**Figure 1.** A schematic view of loop and boundary points during a FFS run. Boundary points (open circles) connect a boundary interface ( $\lambda_{i-1}$  or  $\lambda_{i+1}$ ) with the middle interface ( $\lambda_i$ ). The loop points (filled circles) belong to trajectories that meet first the middle interface in both directions. The dashed lines and crosses correspond to paths that are not sampled during FFS.

trial trajectories from an interface  $\lambda_i$ , and ending when the next interface  $\lambda_{i+1}$  or the basin A (i.e.,  $\lambda_0$ ) is hit. Even though the harvested partial paths started at  $\lambda_i$  are free to follow any possible path between A and  $\lambda_{i+1}$ , including paths crossing previous interfaces several times, this sampling is incomplete because the partial paths reaching  $\lambda_{i+1}$  are stopped and thus not allowed to explore the system in the opposite direction (i.e., unidirectional sampling). Even statistics from partial paths returning to the initial region A introduce a bias, since the  $p_i(\lambda)$  distribution would only contain contributions from trajectories coming from the basin A, missing the contribution from those that originate from basin B. To correct for these biases, a complementary US strategy is performed by accumulating more statistics inside the windows. While this US portion could be done concurrently at each stage of the FFS simulation, for simplicity, we assume here that US run is performed *after* the FFS run has finished. For this purpose, the FFS contribution to  $H_i(\lambda)$ , to be denoted as the histogram  $h_i^{\text{FFS}}(\lambda)$ , must be stored during the FFS run as explained shortly. Hence, the total histogram  $H_i(\lambda)$  is computed by joining  $h_i^{\text{FFS}}(\lambda)$  and an extra US histogram  $h_i^{\text{US}}(\lambda)$ :

$$H_i(\lambda) = h_i^{\text{FFS}}(\lambda) + h_i^{\text{US}}(\lambda) \quad (11)$$

**D.1. Evaluation of  $h^{\text{FFS}}(\lambda)$ .** During the FFS-type simulation, for each trial trajectory initiated at  $\lambda_i$ , statistics of the system's visits inside the boundaries ( $\lambda_{i-1} < \lambda < \lambda_{i+1}$ ) are accumulated until the system reached the  $\lambda_{i-1}$  or  $\lambda_{i+1}$  interface. The collection of all states "visited" by these paths is a subset of the phase space points between  $\lambda_{i-1}$  and  $\lambda_{i+1}$  because the points from trajectories meandering around the outer interfaces are missing. In analogy to the method presented by Moroni et al.,<sup>5</sup> the states along a partial path are categorized as either "loop" or "boundary" points as illustrated in Figure 1. For any given trajectory started at  $\lambda_i$ , the states connecting  $\lambda_i$  and  $\lambda_{i-1}$  are classified as backward boundary points [ $b_{i-i-1}(\lambda)$ ] and the rest of them as loop points [ $l_i(\lambda)$ ]. Likewise, for any given trajectory started at  $\lambda_i$ , the states connecting  $\lambda_i$  and  $\lambda_{i+1}$  are classified as forward boundary points [ $f_{i-i+1}(\lambda)$ ] and the rest of them as loop points [ $l_i(\lambda)$ ]. Any lack of sampling around the outer interfaces can then be made up for by meshing neighboring interface

ensembles as follows. First, note that in steady state the flux of trajectories coming from A and B should be the same; i.e.

$$n_{i \rightarrow i+1} = n_{i+1 \rightarrow i} \quad (12)$$

where  $n_{i \rightarrow i+1}$  is the number of partial paths started at  $\lambda_i$  that meet  $\lambda_{i+1}$  before  $\lambda_{i-1}$ , and  $n_{i+1 \rightarrow i}$  is the number of partial paths started at  $\lambda_{i+1}$  that meet  $\lambda_i$  before  $\lambda_{i+2}$ . Hence, the FFS run contribution to the total  $H_i(\lambda)$  histogram can be estimated by weighing the contributions of neighboring interfaces ensembles to satisfy eq 12; i.e., for points in  $[\lambda_i, \lambda_{i+1}]$  we have

$$h_i^{\text{FFS}}(\lambda) = f_{i \rightarrow i+1}(\lambda) + W_{i-1}[l_i(\lambda)] + W_i[b_{i+1 \rightarrow i}(\lambda) + l_{i+1}(\lambda)] \quad (13)$$

where the scaling factors are defined as  $W_0 = 1$  and  $W_i = n_{i+1 \rightarrow i} / n_{i \rightarrow i+1}$ . The  $W_{i-1}$  term in eq 13 arises from the matching procedure for the loop and boundary point histograms for the previous  $\lambda_{i-1} \leq \lambda \leq \lambda_i$  window. Once all scaling factors ( $W_i$ ) are known, the total histogram  $h_i^{\text{FFS}}(\lambda)$  can be computed by joining all the boundary and loop histograms via eq 13.

**D.2. Evaluation of  $h^{\text{US}}(\lambda)$ .** The US contribution to the total  $H_i(\lambda)$  histogram in the  $w_i$  window ( $\lambda_i \leq \lambda \leq \lambda_{i+1}$ ) is obtained from a conventional US simulation using the interfaces as hard window boundaries ( $\lambda_i$  and  $\lambda_{i+1}$ ) with a weighting function of zero.<sup>4</sup> For each window, this simulation is initiated from  $N_{\text{US}}$  points at interface  $\lambda_i$ , randomly selected from those stored during the FFS run, and continued until eqs 14 and 15 below [which are essentially eqs 8 and 10] are satisfied. Equation 14 is eq 8 suitably modified in account of eq 11:

$$\sum_{\lambda=\lambda_i}^{\lambda_{i+1}} h_i^{\text{US}}(\lambda) \geq N_{\text{win}}^{(i)} - \sum_{\lambda=\lambda_i}^{\lambda_{i+1}} h_i^{\text{FFS}}(\lambda) \quad (14)$$

where  $h_i^{\text{US}}(\lambda) = \sum_{k=1}^{N_{\text{US}}} h_{i,k}^{\text{US}}(\lambda)$  and  $h_{i,k}^{\text{US}}(\lambda)$  is the US histogram registering entries in the  $i$ th window and  $k$ th starting point at  $\lambda_i$ . Equation 15 is eq 10 applied to the US data only:

$$\min[h_{i,k}^{\text{US}}(\lambda)] \geq N_{\text{bin}}, \quad \forall k \quad (15)$$

For simplicity, we used  $N_{\text{US}} = 1$  for the examples in this work. As discussed in section II C,  $N_{\text{bin}}$  is chosen such that the paths sample  $w_i$  long enough to lose “memory” of their starting points, while  $N_{\text{win}}^{(i)}$  is chosen such that the total computational cost to obtain the equilibrium distribution from the FFS-US approach is comparable to that of a conventional US simulation.

The unnormalized distribution inside each window ( $w_i$ ) is simply found from  $p_i(\lambda) = H_i(\lambda) / \sum_{\lambda=\lambda_i}^{\lambda_{i+1}} H_i(\lambda)$ . To obtain the complete  $p(\lambda)$  distribution, we need to employ conventional US calculations to sample the states inside and close to the stable regions A and B where  $p(\lambda)$  can be readily obtained this way. The FFS-US is therefore reserved to sample  $p(\lambda)$  in the barrier region between A and B which is rarely visited by brute-force “BF” simulations (i.e., leading to poor statistics). In practice, performing FFS-US only on a few windows with some overlapping (i.e., if neighboring windows overlap by at least one state) is sufficient to obtain an entire continuous free energy profile in the region  $[\lambda_0, \lambda_{n-1}]$ , as shown in section III.

The contribution to the  $w_i$ 's  $H_i(\lambda)$  from the  $h_i^{\text{FFS}}(\lambda)$  is defined as the ratio

$$R_{\text{FFS}} = \sum_{\lambda=\lambda_i}^{\lambda_{i+1}} h_i^{\text{FFS}}(\lambda) / \sum_{\lambda=\lambda_i}^{\lambda_{i+1}} H_i(\lambda) \quad (16)$$

where the  $h_i^{\text{FFS}}(\lambda)$ 's only include statistics from FFS trajectories that contributed to the  $p(\lambda)$  distribution.  $R_{\text{FFS}}$  can be seen as a

measure of the efficiency of the FFS-US combination since it represents the fractional savings in the length of the standard US simulation that the FFS data provides (the higher the  $R_{\text{FFS}}$ , the higher the efficiency).

It is finally noted that rather than using histogram-based or “visited-states” approach to find the  $p(\lambda)$  distribution [i.e., accumulating histograms for statistics of the frequency with which the system visits  $\lambda$  states] we could employ a transition matrix (TM) method that relies on information on the probabilities of transitioning between  $\lambda$  states.<sup>18</sup> While we did implement such a TM approach (following ref 18) and found its results to agree well with those of visited-states approach, we did not observe any clear advantage of using former and thus we will only report results for the latter.

**E. Multiple State FFS.** In FFS simulations, the rate constant estimation is restricted to pathways connecting two stable states. However, for complex systems the trajectories between two stable states might visit several intermediate states interconnected in phase space. If we are interested in estimating rate constants for all the multiple transitions,  $N(N-1)$  (where  $N$  is the number of metastable states) independent FFS simulations could be performed, but such an approach would be very inefficient. To partially address this problem, we reformulated the FFS formalism to calculate rate constant for all the transitions that connect any two stable states through intermediate states within one single simulation.

In analogy to the method presented by Rogal and Bolhuis,<sup>13</sup> it is assumed that the intermediate states have already been identified and that we can express the rate constant for transitions from state A to B and passing through  $M$  metastable states forming a set  $\mathbf{m}$  (i.e.,  $M \geq 1$ ) as

$$k_{A \rightarrow \mathbf{m} \rightarrow B} = P(\lambda_{n=B} | \lambda_{\mathbf{m}}) k_{A \rightarrow B}^T \quad (17)$$

where  $k_{A \rightarrow B}^T$  is the overall transition rate constant connecting states A and B, and  $P(\lambda_{n=B} | \lambda_{\mathbf{m}})$  is the conditional probability that whenever the interfaces of the intermediate states  $\mathbf{m}$  are crossed by a trajectory coming from A, state B will be reached before returning to A (note that  $\mathbf{m}$  could denote a single or multiple metastable states). The intermediate state crossing probability  $P(\lambda_{n=B} | \lambda_{\mathbf{m}}) = n_{A \rightarrow \mathbf{m}} / N^{(n)}$  is simply given by the number,  $n_{A \rightarrow \mathbf{m}}$ , of pathways starting in A, crossing the intermediate states  $\mathbf{m}$  and ending in B divided by the number of all the pathways,  $N^{(n)}$ , starting in A and reaching B. Equation 17 is further simplified using eq 1 and recalling that for the BG method  $P(\lambda_{n=B} | \lambda_0) = N^{(n-1)} / \prod_{i=0}^{n-1} k_i$

$$k_{A \rightarrow \mathbf{m} \rightarrow B} = \Phi_{A0} \frac{n_{A \rightarrow \mathbf{m}}}{\prod_{i=0}^{n-1} k_i} \quad (18)$$

Once the FFS simulation ends,  $n_{A \rightarrow \mathbf{m}}$  is obtained by tracing back the pathways in the TPE. Since the flux,  $\Phi_{A,0}$ , is constant for all transitions out of state A, the ratio of the two rate constants can be expressed as the ratio of intermediate state crossing probabilities

$$\frac{k_{A \rightarrow \mathbf{m} \rightarrow B}}{k_{A \rightarrow \mathbf{r} \rightarrow B}} = \frac{P(\lambda_{n=B} | \lambda_{\mathbf{m}})}{P(\lambda_{n=B} | \lambda_{\mathbf{r}})} = \frac{n_{A \rightarrow \mathbf{m}}}{n_{A \rightarrow \mathbf{r}}} \quad (19)$$

There are two types of rate constants of particular interest to understand the transition mechanism: (i) Rate constants  $k_{A \rightarrow \mathbf{m}}$  where  $m$  is a single intermediate state visited directly from A; these tell us about the possible destinations of pathways right after leaving A, and (ii) rate constants  $k_{A \rightarrow * \rightarrow \mathbf{m} \rightarrow B}$ , which are instrumental to quantify the immediate sources of trajectories that reach B. Here the star symbol (\*) is used to represent any

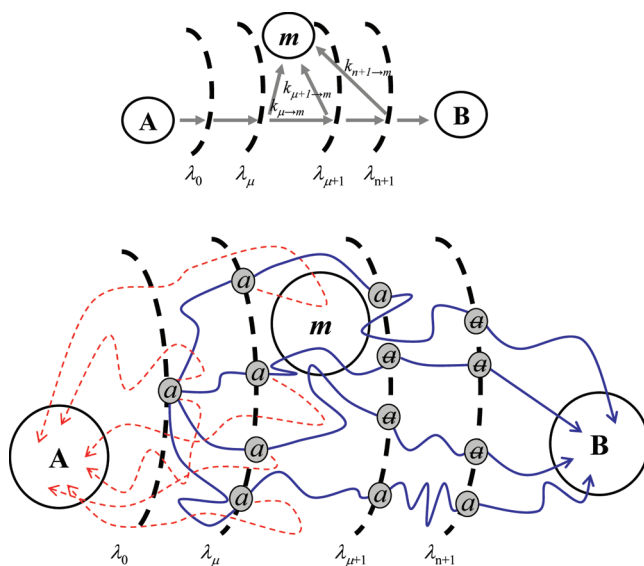


**Figure 2.** Multiple state FFS simulations. (a, top) The overall transition rate constant between the basin A and  $m$  intermediate state,  $k_{A-m}$ , is estimated as resistors in parallel:  $k_{A-m} = k_{\mu-m} + k_{\mu+1-m} + k_{n+1-m}$ . (b, bottom) A schematic view of the “active” ( $a$ ) and “inactive” ( $\alpha$ ) points for the calculation of the rate constants for multiple transitions.

number of possible jumps among different intermediate states, so that  $A \rightarrow * \rightarrow m \rightarrow B$  denotes the transition for all trajectories that started in A, ended in B, and visited intermediate state “ $m$ ” just before ending in B, regardless of whether or not jumps among intermediate states occurred before the  $m \rightarrow B$  step. Note that  $k_{A \rightarrow B} + \sum_{m=1}^M k_{A \rightarrow m}$  is the total rate of leaving A to any other destination, and the total  $A \rightarrow B$  rate constant is  $k_{A \rightarrow B}^T = k_{A \rightarrow B} + \sum_{m=1}^M k_{A \rightarrow * \rightarrow m \rightarrow B}$ , where  $k_{A \rightarrow B}$  is the rate constant associated with direct paths from A to B (without passing through any intermediate).

To evaluate such rate constants as  $k_{A \rightarrow m}$  and  $k_{A \rightarrow * \rightarrow m \rightarrow B}$ , it is convenient to label the stored points as  $\{p,q\}$ , keeping track of the two most recent states visited: “ $q$ ” is the most recent state visited and “ $p$ ” is the one visited before  $q$ . The  $\{p,q\}$  pair is initialized as  $\{a,a\}$  where “ $a$ ” denotes basin A as the origin. State “ $p$ ” could be either another intermediate state ( $p \neq q$ ) or state A ( $p = a$ , when the path went  $A \rightarrow q$  directly). State “ $q$ ” could either be an intermediate state or still be  $q = a$  if no intermediate state has yet been visited. Thus, e.g., if a partial trajectory connects a configuration at  $\lambda_i$  with pair label  $\{p_i, q_i\}$  with a configuration at  $\lambda_{i+1}$  with label  $\{p_{i+1}, q_{i+1}\}$ , then if such partial trajectory visited intermediate state  $m$ , we must have  $p_{i+1} = q_i$  and  $q_{i+1} = m$ ; otherwise the label stays the same (i.e.,  $p_{i+1} = p_i$ ,  $q_{i+1} = q_i$ ).

To evaluate constants  $k_{A \rightarrow m}$ , rather than using separate FFS runs, we can estimate them via a single FFS simulation (connecting stable states A and B) as follows. The stored states at  $\lambda_i$  are categorized as either “active” ( $a$ ) or “inactive” ( $\alpha$ ) points as illustrated in Figure 2b. An active point in one for which the  $\{p,q\}$  label is  $\{a,a\}$ , and is inactive otherwise. Clearly, an “active” point is a state along a partial trajectory that starts in basin A and has not committed yet to any intermediate or stable state. Figure 2a shows schematically that the overall transition rate constant  $k_{A \rightarrow m}$  can then be estimated as the treatment for reactions or resistors in parallel:

$$k_{A \rightarrow m} \approx \sum_{\xi=\mu}^{n-1} k_{\xi \rightarrow m} \quad (20)$$

where  $\xi$  corresponds to the interface index and  $\mu$  is the index of last interface in the phase space immediately prior to the intermediate state  $m$ . To calculate the rate constant between a  $\xi$  interface and intermediate  $m$ ,  $k_{\xi \rightarrow m}$ , we relate it to the conditional probabilities,  $P_a(\lambda_{i+1} | \lambda_i)$ , to reach  $\lambda_{i+1}$  from an “active” configuration at  $\lambda_i$ , as follows

$$k_{\xi \rightarrow m} \approx \frac{n_{\xi \rightarrow m}}{n_a^\xi} \Phi_{A0} \prod_{i=0}^{\xi-1} P_a(\lambda_{i+1} | \lambda_i) \quad (21)$$

where  $n_{\xi \rightarrow m}$  is the number of trial runs fired at  $\lambda_\xi$  that started from any point labeled ( $a$ ) and reached  $m$  before basin A, B, or other intermediate state;  $n_a^\xi = N_a^\xi k_\xi$  is the total number of fired trial runs at  $\lambda_\xi$  from ( $a$ ) points, where  $N_a^\xi$  is the number of ( $a$ ) points at  $\lambda_\xi$ . In eq 21,  $P_a(\lambda_{i+1} | \lambda_i) = N^{(i+1)} / n_a^i$ , where  $N^{(i+1)} = N_a^{(i+1)} + N_a^{(i+1)}$  is the number of trial runs reaching  $\lambda_{i+1}$ .

To evaluate rate constants  $k_{A \rightarrow * \rightarrow m \rightarrow B}$ , we can use the  $\{p,q\}$  labels described above and apply eq 18 by simply tracing back the TPE pathways of type  $\{p,q\}$  where  $q = m$  and  $p$  is any state; i.e.,  $k_{A \rightarrow * \rightarrow m \rightarrow B} = \Phi_{A0} [n_{A \rightarrow * \rightarrow m \rightarrow B} / \prod_{i=0}^{n-1} k_i]$ , where  $n_{A \rightarrow * \rightarrow m \rightarrow B}$  is the total number of such paths. Likewise, for  $k_{A \rightarrow m \rightarrow B}$  and  $k_{A \rightarrow B}$  one would simply use the paths (from those that reached B) with label  $\{a,m\}$  and  $\{a,a\}$ , respectively.

While eqs 18 and 21 were derived adapting some of the concepts of the multiple state transition path method of Rogal and Bolhuis,<sup>13</sup> their method allows the calculation of rates for all possible transitions within the phase space including those between intermediate states (like  $k_{m_1 \rightarrow m_2}$ ) and backward from B to A. This is not possible from a single FFS simulation which is unidirectional by design.

### III. Results

**A. Example 1: Lattice Protein Folding.** The protein model adopted here consists of a 48 amino acid sequence that has a unique, compact native structure, whose energy is minimum  $E_{\min} = -20.24k_B T$  with NNC = 57 specific or “native” segment–segment contacts. Further details on the model protein, including its sequence, structure, thermodynamics, and kinetic behavior are given elsewhere.<sup>19,20</sup> The folding kinetics and thermodynamic of the system (via FFS-US) were simulated in free space at the corresponding *bulk transition temperature*  $T_f = 0.27$ .<sup>19,20</sup> Recently, we showed that for this simple system, an order parameter model with linear terms for the number of native contacts (NC) and the configurational energy ( $E$ ) variables:

$$\lambda(\text{NC}, E) = p_B(\text{NC}, E) = -0.404 + 0.017(\text{NC}) - 0.029(E) \quad (22)$$

is a good estimate for the reaction coordinate that describes the dynamical bottleneck between the folded and unfolded stable states.<sup>11,12</sup> Furthermore, this model projects the committor probability ( $p_B$ ) surface on the phase space, i.e., it estimates the probability of any interfacial point stored in the TPE trajectories to commit to the folded state from their NC and  $E$  values. Equation 22 was then used as order parameter to partition the phase space between the unfolded and folded states for the FFS-US simulations, with seven interfaces ( $n = 7$ ) positioned at  $\lambda_i$  ( $0 \leq i \leq n$ ):  $\lambda(x) = \{0, 0.0, 0.1, 0.2, 0.3, 0.5, 0.7, 0.9, 1.0\}$ . The phase space region A was defined by taking  $\lambda \leq 0$  and B by  $\lambda \geq 1.0$ . The calculations were carried out using the DFFS scheme with the number  $M$  of trials at each interface fixed to  $M_i = 100$

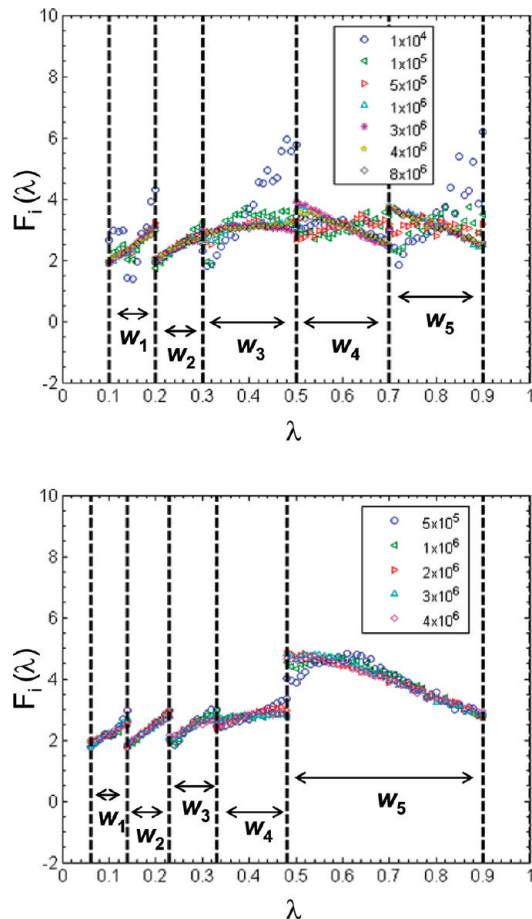


**Figure 3.**  $F_i(\lambda)$  functions from standard US simulations of the protein system in different windows for different values of  $N_{\text{win}}^{(i)}$  and for (a, top) unoptimized and (b, bottom) optimized  $\lambda$  staging. The thick lines correspond to the windows' walls.

( $0 \leq i < n$ ) and with starting points randomly sampled from inside the region A.

First, we investigate if our estimate for the maximum number of entries accumulated for each window  $w_i$ 's histogram ( $N_{\text{win}}^{(i)}$ ) (via eq 5) is valid such that enough visits are accumulated for the  $w_i$ 's  $H_i(\lambda)$  to produce the correct  $F_i(\lambda)$  function. For this purpose, we performed a series of conventional umbrella sampling (US) simulations with different  $N_{\text{win}}^{(i)}$  values for each of the windows shown in Figure 3a. The phase space between the stable states A and B was subdivided into five different window sizes  $[\lambda_i, \lambda_{i+1}]$ , overlapping each other by one state. The US simulations were initiated from a randomly selected state at interface  $\lambda_i$ . In Figure 3a, we compare the  $F_i(\lambda)$  functions in different windows obtained with different  $N_{\text{win}}^{(i)}$  values. Note that the minimum  $N_{\text{win}}^{(i)}$  value which produce the correct  $F_i(\lambda)$  increases with the  $w_i$ 's size, for example,  $N_{\text{win}}^{(i)} \sim 10^5$  MC steps for  $w_1$  and  $w_2$  and  $N_{\text{win}}^{(i)} \sim 4 \times 10^6$  for  $w_3, w_4$ , and  $w_5$  ( $w_3 = w_4 = w_5 > w_1 = w_2$ , where  $w$  stands for the window's width). To verify these results, we also consider a subdivision into five windows, resulting from the phase space partition using an optimized  $\lambda$  staging, as shown in Figure 3b. The optimized  $\{\lambda'\}$  set was found by an adaptive optimization algorithm,<sup>12</sup> which seeks to allocate the computational effort in a FFS simulation to reduce the statistical error with which the reaction rate constant is estimated. The optimized  $\{\lambda'\}$  set corresponds to  $\lambda_i$  ( $0 \leq i \leq n = 7$ ):  $\lambda(x) = \{0.0, 0.06, 0.14, 0.23, 0.33, 0.48, 0.9, 1.0\}$  and the region A and B were defined as before by taking  $\lambda \leq 0$  and  $\lambda \geq 1.0$ , respectively. Again, the minimum  $N_{\text{win}}^{(i)}$  value

**TABLE 1: Data for FFS-US Protein Folding Simulations Using an “Unoptimized”  $\lambda$  Staging<sup>a</sup>**

$w_i [\lambda_i, \lambda_{i+1}]$	$\lambda_i$	$\lambda_{i+1}$	$N_{\text{win}}^{(i)} [\text{MC steps}]$	% $R_{\text{FFS}}$
1	0.10	0.20	$4.21 \times 10^6$	62
2	0.20	0.30	$4.21 \times 10^6$	48
3	0.30	0.50	$1.68 \times 10^6$	19
4	0.50	0.70	$1.68 \times 10^6$	39
5	0.70	0.90	$1.68 \times 10^6$	72

<sup>a</sup> The  $\lambda$  range was subdivided into five US windows  $w_i$ .  $N_{\text{bin}} = 10^4$  and the contribution to each window's  $H_i(\lambda)$  from the FFS-type sampling  $h_i^{\text{FFS}}(\lambda)$  (%  $R_{\text{FFS}}$ ) was determined from 100 DFFS sampling blocks, each one started from a randomly selected point at  $\lambda_0$ .

**TABLE 2: Data for the FFS-US Protein Folding Simulations Using the Optimized  $\lambda$  Staging, and Five US Windows  $w_i^a$**

$w_i [\lambda_i, \lambda_{i+1}]$	$\lambda_i$	$\lambda_{i+1}$	$N_{\text{win}}^{(i)} [\text{MC steps}]$	% $R_{\text{FFS}}$
1	0.06	0.14	$1.7 \times 10^5$	52
2	0.14	0.23	$2.1 \times 10^5$	46
3	0.23	0.33	$2.6 \times 10^5$	61
4	0.33	0.48	$5.9 \times 10^5$	50
5	0.48	0.90	$4.6 \times 10^6$	33

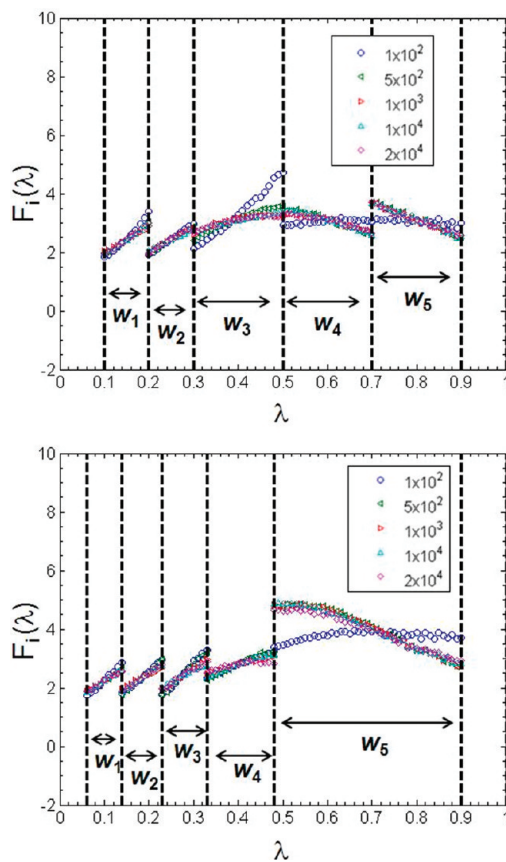
<sup>a</sup>  $N_{\text{bin}} = 10^4$  and the contribution to each window's  $H_i(\lambda)$  from the FFS-type sampling  $h_i^{\text{FFS}}(\lambda)$  (%  $R_{\text{FFS}}$ ) was determined from 100 DFFS sampling blocks, each one started from a randomly selected point at  $\lambda_0$ .

which produces the correct  $F_k(\lambda)$  increases with the  $w_i$ 's size, for example,  $N_{\text{win}}^{(i)}$  is of order  $\sim 10^5$  and  $4 \times 10^6$  MC steps for  $w_1$  and  $w_5$  ( $w_5 > w_1$ ), respectively.

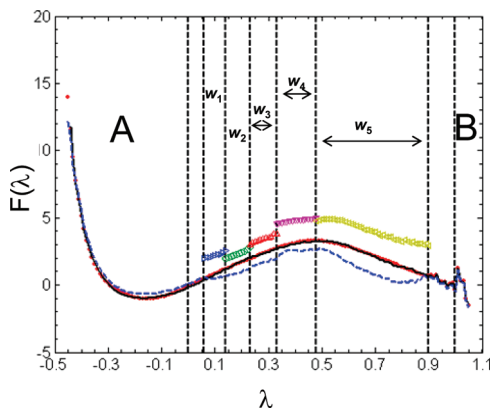
Tables 1 and 2 give the  $N_{\text{win}}^{(i)}$  values in each  $w_i$  [ $\lambda_i, \lambda_{i+1}$ ] estimated by eq 5, where the constant  $a$  was calculated for five windows ( $m = 5$ ) and assuming that the total computational time spent by a standard brute force (BF) simulation in that region [ $\lambda_1 = 0.06, \lambda_6 = 0.9$ ] is approximately  $t_{\text{CPU}} = 3 \times 10^7$  MC steps. Equations 6 and 7 predicted that the total computational cost to obtain the  $p(\lambda)$  distribution from the FFS-US approach is  $\tau \approx 5.9 \times 10^6$  MC steps, and the constant  $a$  is equal to  $4.2 \times 10^3$  and  $2.6 \times 10^3$  MC steps for the “unoptimized” and optimized  $\lambda$  staging simulations, respectively. Note in Tables 1 and 2 that for all  $w_i$  the estimated  $N_{\text{win}}^{(i)}$  values are of the same order as the values predicted by the conventional US simulations in Figure 3.

Figure 4, a and b, shows the  $F_i(\lambda)$  functions in different windows obtained with different values of the minimum number of statistics per bin,  $N_{\text{bin}}$ , for the “unoptimized” and optimized  $\lambda$  staging simulations, respectively. Note that the  $F_i(\lambda)$  functions were estimated by accumulating statistics in  $H_i(\lambda)$  from several partial paths, each of them allowed to explore the  $w_i$ 's region until the condition (15) is met. The number of trial paths ( $M_i$ ) that are sampling the  $w_i$  and contribute to  $h_i^{\text{FFS}}(\lambda)$  was constrained by the condition (14) ( $N_{\text{win}}^{(i)}$  values are given in Tables 1 and 2). For example, as expected, the  $N_{\text{bin}}$  value which produces the correct  $F_k(\lambda)$  is of order  $\sim 5 \times 10^2$  and  $10^3$  MC steps for  $w_1$  and  $w_5$  ( $w_5 > w_1$ ), respectively (see section IIB). Thus, the contribution to the statistical error ( $\delta$ ) in  $p_i(\lambda)$  from just one partial path is of order  $\Delta_k \sim O(0.04$  and  $0.03)$  for the  $w_1$  and  $w_5$  ( $w_5 > w_1$ ), respectively. Therefore, for this system we assumed that at each  $w_i$  a partial trajectory lost its “memory” during a sampling time not much longer than the time required to accomplish condition (15) where  $N_{\text{bin}}$  is of order  $\sim 10^4$  MC steps.

In Figure 5 we show results for the free energy profile obtained from the simulations in each of the five windows in Table 2. The free energy in the stable regions A and B was



**Figure 4.**  $F_i(\lambda)$  functions from FFS-US simulations of the protein system in different windows for different choices of  $N_{\text{bin}}$  and for (a, top) unoptimized and (b, bottom) optimized  $\lambda$  staging. The thick lines correspond to the US windows' walls.



**Figure 5.** Sequence of measured free energies  $F(\lambda)$  from the FFS-US simulations for the protein system. The continuous  $F(\lambda)$  function was obtained after fitting the results for the  $F_i(\lambda)$  in the different windows (red dot). The DFFS scheme was used with an optimized  $\lambda$  staging. The  $\lambda$  staging for the FFS-US simulation is shown by dotted lines. The free energy in the stable regions A and B was obtained by directly histogramming  $P(\lambda)$  by means of two standard US simulations. Results from a standard US simulation over the entire domain are also shown (dark line). The free energy profile obtained from the FFS histogram  $h_i^{\text{FFS}}(\lambda)$  is also shown.

obtained by directly histogramming  $p(\lambda)$  by means of two US standard simulations. Note, however, that the histogram  $H_A(\lambda)$  for stable state A ( $\lambda \leq \lambda_0$ ) could be obtained from the flux term estimation in eq 1 (i.e., step one in section II B) when the length of the simulation in the basin A is long enough. The continuous free energy profile was then calculated according to eq 4 and compared to the results of a standard BF simulation; Figure 5

shows that these two profiles agree well. The  $F(\lambda)$  function obtained from the FFS histogram  $h_i^{\text{FFS}}(\lambda)$  is also illustrated in Figure 5, showing that the associated  $p_i(\lambda)$  distribution is biased. The extra US data corrects for the bias by sampling regions in the phase space not visited by the trajectories contained in the TPE.

As expected, the stagewise nature of FFS-US leads to a reduction in the computational effort to obtain the  $p(\lambda)$  distribution by a factor of  $m = 5$  (compared to the cost of a standard BF simulation). Tables 1 and 2 give values for  $R_{\text{FFS}}$  from eq 16 for the five  $w_i$ . Note that  $R_{\text{FFS}}$ , the fractional contribution of  $h_i^{\text{FFS}}(\lambda)$  to the  $w_i$ 's  $H_i(\lambda)$ , varies from 20% to 70%, implying significant savings in computer time.

**B. Example 2: Potential Surface 1.** At least three main challenges have been identified for the application of FFS to the simulation of rare events:<sup>11,12</sup> (1) determination of an adequate order parameter (or combination of parameters) that allows the description of multiple transition state regions of a system; (2) assessing high efficiency and completeness of sampling; and (3) estimation of the free energy landscape (i.e., stationary distributions) and barriers. In a previous work,<sup>11</sup> we addressed the first challenge by proposing a new algorithm, FFS-LSE, for identifying suitable reaction coordinates to describe the progression of rare events in complex systems. FFS-LSE uses the transition path ensemble (TPE) obtained from FFS to obtain “on-the-fly” estimates of the committor probability to the final region,  $p_B$ , to screen out good order parameter models. More recently,<sup>12</sup> we addressed the second challenge by applying an adaptive algorithm which reduces the statistical error of the estimated transition rate constant (for a given computational cost) by optimizing either the number of trial runs per interface (for fixed staging) or the staging (for fixed interface sampling). We now propose to address the third challenge by the use of the FFS-US algorithm. In this and the following section, we use all these algorithms to study the diffusion of a particle on a two-dimensional rugged energy surface that is representative of systems with multiple barriers (i.e., metastable states) encountered in many applications.

The model surface under study was used by Chopra et al.<sup>21</sup> and consists of a sum of overlapping Gaussians: 9 major and 100 minor random surfaces. The major surfaces exhibit two well-defined global minima at  $(x,y) = (0.2, 0.2)$  and  $(0.8, 0.8)$  (i.e., A and B stable states, respectively) and three local minima at  $(0.14, 0.88)$ ,  $(0.35, 0.75)$ , and  $(0.8, 0.2)$  which correspond to metastable states. To these major features, 100 random Gaussians are superimposed to increase the roughness of the potential surface. A contour graph of this energy landscape showing the A and B basins is illustrated in Figure 6. The initial region was defined by the square region enclosed by  $0.1 \leq x \leq 0.3$  and  $0.1 \leq y \leq 0.3$ . The final region was defined by a square region enclosed by  $0.7 \leq x \leq 0.9$  and  $0.7 \leq y \leq 0.9$ . The time evolution of the system was simulated using Brownian dynamics at  $\beta = 1/k_B T = 0.5$ . The parameters that describe the particle diffusion on the surface through Langevin dynamics were as follows: time step  $\Delta t = 0.01$ , mass  $m = 1.0$ , and friction coefficient  $\gamma = 2.5$ . Reflective boundaries were enacted by reflecting the particle moves at the edges with  $x$ ,  $y$ -coordinate  $< 0$  and  $x$ ,  $y$ -coordinate  $> 1$ . Figure 6 also illustrates the initial  $\lambda$  staging:  $\lambda_i = x$ -coordinate for  $0 \leq i < n$  was used as initial guess of order parameter. The  $\lambda$  space was partitioned into  $n = 9$  interfaces positioned at  $\lambda_i$  ( $0 \leq i < n$ ):  $\lambda(x) = \{0.31, 0.32, 0.34, 0.36, 0.40, 0.45, 0.50, 0.55, 0.65\}$  and  $\lambda_{n=9}$  was taken as the square region

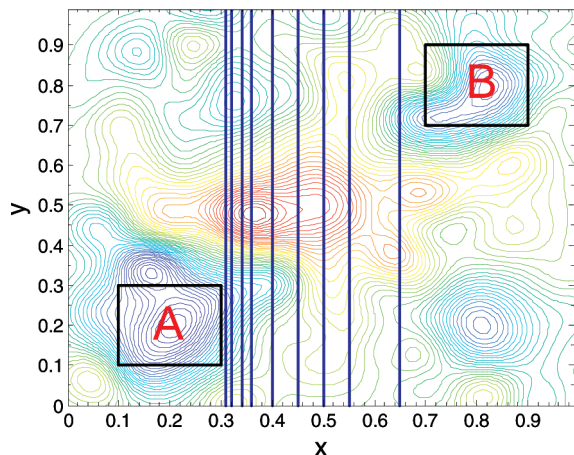


**Figure 6.** Contour graph of the free-energy surface for the two-dimensional potential no. 1.<sup>21</sup> The color scheme changes from highest (red) to lowest (blue) elevations. The initial and final regions are shown by the squares labeled A and B, respectively. The initial  $\lambda$  staging for the FFS-type simulation is shown by solid vertical lines (blue).

enclosing the stable state B. The number of trials per point at  $\lambda_i$  for the BG method was  $k_0 = 200$  ( $i = 0$ ) and  $k_i = 10$  ( $1 \leq i < n$ ).

Figure 7a shows a map of the probability density ( $P_{\text{TPE}}$ ) of finding a configuration  $(x, y)$  in the TPE after a long FFS run [ $P_{\text{TPE}}(x, y)$  is incremented by one if a  $A \rightarrow B$  trajectory visits this configuration at least once], where it can be seen that the trajectories connecting the two stable states A and B visit the three metastable states with similar frequency. However, Figure 7b shows that the free energy profile  $F(\lambda=x)$  along this initial guess of order parameter exhibits only two stable states (wells), i.e., the metastable states at the local minima (0.14, 0.88) and (0.35, 0.75) overlap with state A, while the metastable state at (0.8, 0.2) overlaps with state B.

We now explore the possibility that our FFS-LSE method and a staging optimization could help us estimate a good reaction coordinate for this system, allowing a higher computational efficiency for the FFS simulation and the identification of the multiple barriers in the transition. The calculations were carried out with the BG method as a series of blocks, each block consisting of 10 runs, each one started from a randomly selected configuration at  $\lambda_0$  (out of  $N_0 = 1000$  points generated at  $\lambda_0$ ) from which a branched path is generated and used to estimate committor probabilities  $p_B$ . The  $p_B$  history data is obtained over ten blocks. Following the FFS-LSE protocol, the  $p_B$  value for every interfacial point stored in the TPE trajectories was obtained by using recursively eq 5 from ref 11. Because  $p_B$  is the ideal reaction coordinate, a good order parameter model will be one that is able to “fit” well these  $p_B$  data.<sup>22,23</sup> To find such a model, one assumes that  $p_B$  follows a mathematical relation (with linear coefficients) that depends on any number of candidate collective properties suspected to be meaningful order parameters; the unknown coefficients are then found by standard least-squares estimation (LSE) and the statistically significant terms in the model are found by analysis of variance. The readers are referred to ref 11 for more details of the FFS-LSE method. Between blocks, our adaptive optimization algorithm<sup>12</sup> was applied to find a better  $\lambda$  staging of the order parameter as follows. The conditional probabilities  $P(\lambda_{i+1}|\lambda_i)$  to reach subsequent interfaces were tracked to identify “bottlenecks” where sampling should be concentrated by restaging. This is done by “interpolating” from the current  $P(\lambda_{i+1}|\lambda_i)$  vs  $\lambda$  data [via an auxiliary function defined by eq 40 in ref 12] to find a new

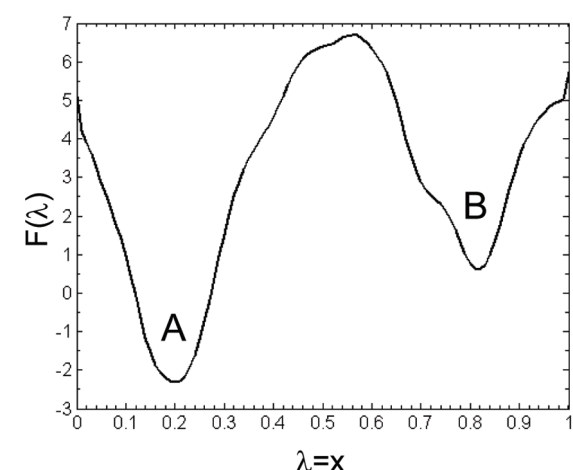
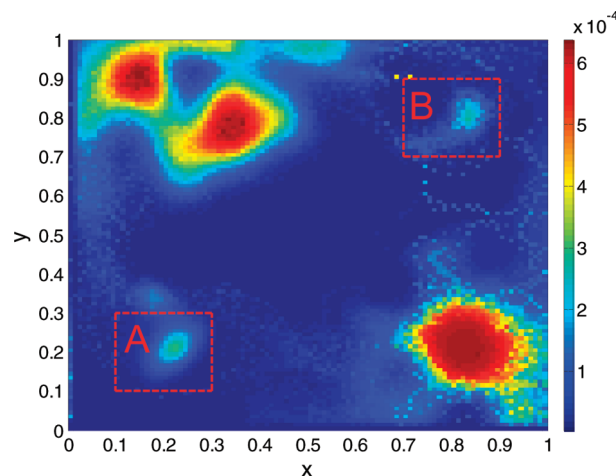


**Figure 7.** Results for the potential energy surface system. (a, top) Density map ( $P_{\text{TSE}}$ ) obtained from the TPE after a long FFS run. (b, bottom) Free energy  $F(\lambda=x)$  profile along the  $x$  coordinate as reaction coordinate.

$\{\lambda'\}$  set for which the  $P(\lambda_{i+1}|\lambda_i)$  values have some prespecified, desired values [e.g.,  $P(\lambda_{i+1}|\lambda_i) = [P(\lambda_n|\lambda_0)]^{1/n} = \text{constant}$ ]. The readers are referred to ref 12 for a detailed description of the adaptive optimization algorithm. This combination of FFS-LSE and staging optimization provides the advantage of allowing a more efficient and uniform distribution of the  $p_B$  data over all the phase space.

Coming back to the present case, the  $p_B$  data thus collected were fitted to a tentative regression model that included two collective variables:  $x$ -, and  $y$ -coordinate, and interaction terms between these variables. Table 3 shows the parameters for reaction coordinate models obtained from the iterations of the combined scheme (i.e., FFS-LSE and adaptive optimization algorithm). For the first iteration, the LSE and analysis of variance for this reaction coordinate model (i.e., model 1 in Table 3) indicated that the linear terms for  $x$ -, and  $y$ -coordinate are the only significant ones. The  $p_B$  surface predicted by this reaction coordinate model (model 1 in Table 3) is illustrated in Figure 8a (dotted lines). A second iteration was performed using this new estimate of order parameter and  $n = 9$  interfaces initially positioned at  $\lambda_i$  ( $0 \leq i < n$ ):  $\lambda(x,y) = \{0.0, 0.1, 0.2, 0.3, 0.4, 0.5, 0.6, 0.7, 0.8\}$ . The stable states A and B were defined as before. The number of trials per point at  $\lambda_i$  for the BG method was  $k_0 = 200$  ( $i = 0$ ) and  $k_i = 10$  ( $1 \leq i < n$ ). Note that while we used three iterations to ensure full convergence, two iterations were enough to get suitable convergence. The  $p_B$

**TABLE 3: FFS-LSE Parameters for the 2D Potential Energy Surface No. 1 Reaction Coordinate Model**  $p_B \approx \beta + \beta_x x + \beta_y y + \beta_{xy} xy + \beta_{xx} x^2 + \beta_{yy} y^2 + \beta_{xxx} x^3 + \beta_{yyy} y^3 + \beta_{xxy} x^2 y + \beta_{xyy} x y^2$ 

model	constant ( $\beta_0$ )	model coefficient ( $\beta$ )								
		x	y	xy	$x^2$	$y^2$	$x^3$	$y^3$	$x^2 y$	$x y^2$
1	-0.55	1.16	0.72	—	—	—	—	—	—	—
2	-0.11	-0.80	-1.29	-0.37	5.17	5.50	-3.72	-3.67	—	—
3	0.20	-1.68	-1.78	-0.06	6.06	6.25	-4.10	-4.17	—	—

**TABLE 4: Data for the FFS-US Simulations with Energy Potential Surface No. 1 and Four Windows Dividing the Phase Space between Stable States<sup>a</sup>**

$w_i [\lambda_{i-1}, \lambda_{i+1}]$	$\lambda_i$	$\lambda_{i+1}$	$N_{\text{win}}^{(i)} [\Delta t]$	% $R_{\text{FFS}}$
1	0.10	0.18	$4.9 \times 10^6$	50
2	0.18	0.27	$6.3 \times 10^6$	15
3	0.27	0.35	$4.9 \times 10^6$	90
4	0.35	0.90	$2.3 \times 10^8$	60

<sup>a</sup>  $N_{\text{bin}} = 5 \times 10^3$  and %  $R_{\text{FFS}}$  was determined from 10 BG sampling blocks, each one started from 10 randomly selected points at  $\lambda_0$ .

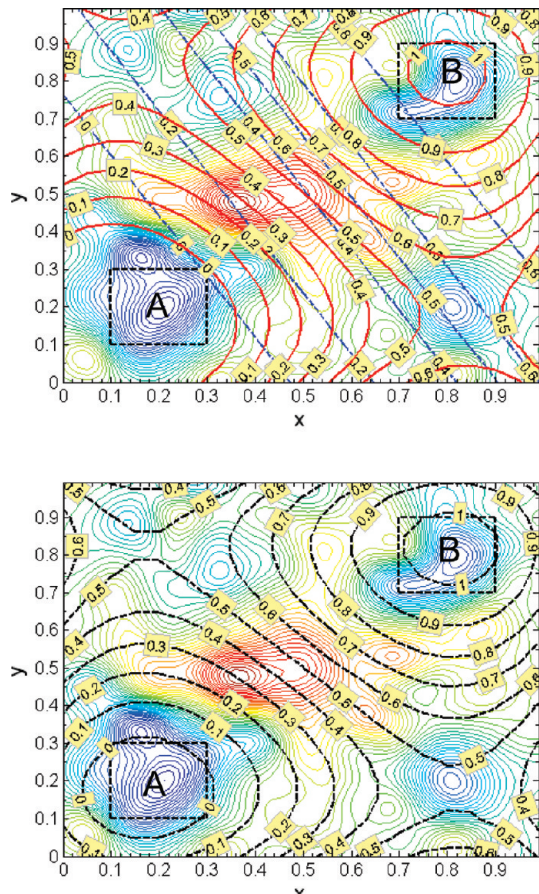


**Figure 8.** Estimated reaction-coordinate iso-lines for the 2D potential energy surface no. 1. (a, top) Thin dotted (blue) and solid (red) lines are the predicted  $p_B$  committors from models 1 and 2 in Table 3, respectively. (b, bottom) The dotted lines (black) are the predicted  $p_B$  committors from model 3 in Table 3. The committer values are shown as labels. Contour plot of the free energy landscape is shown as background for visual reference and the color scheme changes from highest (red) to lowest (blue) elevations. The initial and final regions are shown by the squares labeled A and B, respectively.

surface predicted by the reaction coordinate model estimated from the second and third iterations (models 2 and 3 in Table 3) are illustrated in Figures 8a (solid lines) and 7b (dotted lines). The coefficients (and  $p_B$  surface) in models 2 and 3 are not

identical but similar and include significant linear, quadratic, and cubic terms for  $x$  and  $y$ .

Model 3 was then used as order parameter to partition the phase space between the A and B states for the FFS-US simulations; with eight interfaces ( $n = 8$ ) positioned at  $\lambda_i$  ( $0 \leq i \leq n$ ):  $\lambda(x) = \{0.0, 0.05, 0.07, 0.10, 0.18, 0.27, 0.35, 0.9, 1.0\}$ . Region A was defined by taking  $\lambda \leq 0$  and region B by  $\lambda \geq 1.0$ . Note that this  $\lambda$  staging corresponds to the optimized  $\{\lambda'_i\}$  set obtained by distributing the  $P(\lambda_{i+1}|\lambda_i)$  values  $P(\lambda_{i+1}|\lambda_i) = P_\lambda$  for  $0 \leq \lambda_i \leq 6$ , where  $P_\lambda = [P(\lambda_{n=8}|\lambda_0)/\prod_{i=1}^{n-1} P(\lambda_{i+1}|\lambda_i)]^{1/7} \approx 0.31$  and  $P(\lambda_8|\lambda_7) = 0.9$  for  $\lambda_7$ ; this guarantees that the seventh interface is placed in the region close to the basin of attraction B and that  $w_7$  (i.e., the last window) encloses the entire phase space region between the transition state (TS) and the region close to basin B ( $\lambda_{n=8(B)} \geq 1.0$ ), as seen in Figure 9. The calculations were carried out using the BG scheme with  $k_0 = 200$  ( $i = 0$ ) and  $k_i = 10$  ( $1 \leq i < n$ ). Table 4 gives the  $w_i$ 's size and its corresponding  $N_{\text{win}}^{(i)}$  values estimated by eq 5, where the constant  $a$  was estimated for four windows ( $m = 4$ ) and assuming that the total computational time required by a standard BF simulation in that region [ $\lambda_3 = 0.10, \lambda_7 = 0.90$ ] is approximately  $t'_{\text{CPU}} = 1 \times 10^9 \Delta t$ . Equations 6 and 7 predicted that the total computational cost to obtain the  $p(\lambda)$  distribution from the FFS-US approach is  $\tau \approx 2.5 \times 10^8 \Delta t$ , and that the constant  $a$  is  $\sim 7.7 \times 10^4 \Delta t$ . The continuous free energy  $F(\lambda)$  profile along the reaction coordinate model 3 using a standard BF simulation of length  $2 \times 10^9 \Delta t$  is shown in Figure 9. The resulting  $\lambda$  staging and the windowing of the phase space for the FFS-US simulation are also illustrated in Figure 9. Excellent agreement is obtained between the results of the FFS-US and BF calculations. The free energies in the stable regions A and B were obtained by directly histogramming  $H_A(\lambda)$  for ( $\lambda \leq \lambda_1$ )

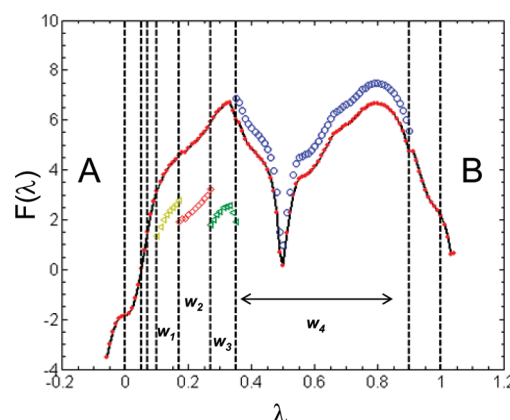


**Figure 9.** Sequence of measured free energies  $F(\lambda)$  along reaction coordinate model 3 (see Table 3) from the FFS-US simulations for the 2D potential energy surface no. 1. The FFS-US  $\lambda$  windows are marked by dotted lines and the partial  $F(\lambda)$  curves in those windows are stitched up together into a continuous  $F(\lambda)$  function shown (red dot). The free energy of the initial and final regions (labeled A and B, respectively) was obtained via standard US simulations. The  $F(\lambda)$  function from a standard brute force simulation is also shown (solid black line).

and  $H_B(\lambda)$  for  $(\lambda \geq \lambda_7)$  during the flux term estimation in eq 1 and a standard BF simulations in the region B, respectively. Note that the  $F(\lambda)$  profile along the reaction coordinate model 3 now shows the two stable states A and B separated by a local minimum at  $\lambda(x,y) = p_B = 0.5$  and two barriers of similar height; this local minimum pools together (in 1D) the three metastable states of the 2D surface. In getting  $p(\lambda)$ , the computational effort is reduced  $\sim m = 4$  fold due to staging (compared to that of a standard BF simulation), and  $h_i^{\text{FFS}}(\lambda)$  contributes from 15% to 90% of the data (see %  $R_{\text{FFS}}$  in Table 4).

Although the multiple state FFS algorithm of section IIIE could be used here to estimate rate constants for some of the intermediate transitions, we restrict such calculations to the following example for which our estimates can be directly compared with previous literature results.

**C. Example 3: Potential Surface 2.** In this section, we also study the diffusion of a particle on a two-dimensional energy surface with multiple metastable states. In contrast to the previous example (section IIB), the trajectories contained on the TPE and connecting both stable states A and B in phase space visit two intermediate states with different frequency, and the surface outside the stable and metastable states is smooth rather than rugged. Besides showing the validity of FFS-US, this example will show that the FFS-LSE derived reaction coordinate allows the identification of the multiple intermediate states in the transition region and the sampling of pathways that connect any two stable or intermediate states (from which rate constants of all possible transitions can be estimated). The model surface is described in detail in ref 13. Figure 10a shows a contour graph of the energy landscape showing the two well-defined global minima at  $(x,y) = (-4,0)$  and  $(4,0)$  (i.e., stable states A and B, respectively) and two local minima at  $(-3,4.8)$  and  $(-0.5,3.2)$  (i.e., metastable states I and II, respectively). The four minima basins are enclosed by circles around the minima with a radius  $r_i$  set to a  $r_A = r_B = 1.0$  and  $r_I = r_{II} = 0.5$ . The time evolution of the system was simulated using Brownian dynamics at  $\beta = 1/k_B T = 2.5$ . The parameters that describe the particle diffusion on the surface through Langevin dynamics were as follows: time step  $\Delta t = 0.1$ , mass  $m = 1.0$ , and friction coefficient  $\gamma = 2.5$ . Reflective boundaries were enacted to keep the particle inside  $-8 < x < 8$  and  $-4 < y < 8$ .

Figure 10b shows a map of the probability density [ $P_{\text{TPE}}(x,y)$ ] of finding a configuration  $(x,y)$  in the TPE after a long FFS run, where it can be seen that the trajectories connecting the two stable states A and B visit the two metastable states with different frequency. Figure 11a shows that the free energy profile  $F(\lambda=x)$  along the  $x$ -coordinate as order parameter exhibits only three wells: the stable states A and B, and the intermediate state II; the metastable states I is not well-defined along this order parameter. To implement the FFS-LSE method, we used the  $x$ -coordinate as initial guess of order parameter, the  $\lambda$  space was partitioned into  $n = 9$  interfaces positioned at  $\lambda_i$  ( $0 \leq i \leq n - 1$ ):  $\lambda(x) = \{-3, -2.5, -2, -1.5, -1, -0.5, 0, 1, 2\}$ , and  $\lambda_{n=9}$  was taken as the circular region enclosing state B. For the BG runs,  $k_0 = 200$  ( $i = 0$ ),  $k_i = 10$  ( $1 \leq i \leq n$ ) and the calculations were carried out as a series of blocks, each one consisting of 10 BG runs. Between blocks, our adaptive optimization algorithm<sup>12</sup> was applied to find a better  $\lambda$  staging of the order parameter as described in the section IIB. Figure 10b also shows isosurfaces for the reaction coordinate obtained from the  $p_B$  data collected after two iterations of the combined scheme and fitted to a tentative regression model that included the  $x$  and  $y$  coordinates and their quadratic and cubic interaction terms; the resulting

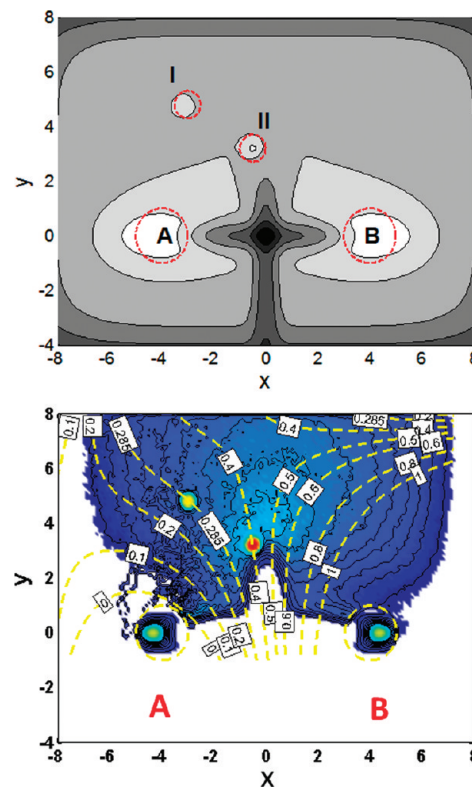


**Figure 10.** (a, top) Contour graph of the free-energy surface for the two-dimensional potential no. 2.<sup>13</sup> The color scheme changes from highest (gray) to lowest (white) elevations. The basins are shown by the cycles labeled A, B, I, and II. (b, bottom) Density map ( $P_{\text{TSE}}$ ) obtained from the TPE after a long FFS run and the predicted  $p_B$  committors (dotted lines, yellow) from the reaction coordinate model found by FFS-LSE; committor values are shown as labels. The color scheme changes from highest (red) to lowest (blue) densities. The initial and final regions are shown by the circles labeled A and B, respectively.

model is  $p_B \approx 0.4151 + 0.2402x + 0.0287y - 0.0330xy + 0.0289x^2 - 0.0039y^2 + 0.0005x^3 - 0.0042x^2y$ .

The optimized order parameter model was then used to partition the phase space between the A and B states for the FFS-US simulations; with nine interfaces ( $n = 9$ ) positioned at  $\lambda_i$  ( $0 \leq i \leq n - 1$ ):  $\lambda(x) = \{0.0, 0.05, 0.10, 0.20, 0.30, 0.40, 0.50, 0.60, 0.9\}$ . Regions A and B were defined by circular regions enclosing the stable A and B minima, respectively. The calculations were carried out using the BG scheme with  $k_0 = 200$  ( $i = 0$ ) and  $k_i = 10$  ( $1 \leq i \leq n$ ). Table 5 gives the  $w_i$ 's size and its corresponding  $N_{\text{win}}^{(i)}$  values estimated by eq 5, where the constant  $a$  was estimated for seven windows ( $m = 7$ ) and assuming that the total computational time required by a standard BF simulation in that region [ $\lambda_1 = 0.05, \lambda_8 = 0.90$ ] is approximately  $t_{\text{CPU}} = 10^9 \Delta t$ . Equations 6 and 7 predicted that  $\tau \approx 1.4 \times 10^7 \Delta t$ , and  $a$  is  $\sim 9.8 \times 10^3 \Delta t$ . The continuous free energy  $F(\lambda)$  profile along the optimum reaction coordinate model using a standard BF simulation of length  $2 \times 10^9 \Delta t$  is shown in Figure 11b. The resulting  $\lambda$  staging and the windowing of the phase space for the FFS-US simulation are also illustrated in Figure 11b. Excellent agreement is obtained between the results of the FFS-US and BF calculations. The free energy in the stable regions A and B were obtained by directly histogramming  $H_A(\lambda)$  for  $(\lambda \leq \lambda_1)$  and  $H_B(\lambda)$  for  $(\lambda \geq \lambda_8)$  during the flux term estimation in eq 1 and a standard BF simulation in the region B, respectively. Note in Figure 11b that the  $F(\lambda)$  profile along the optimized reaction coordinate model now shows the two states A and B separated by two local minima at  $\lambda(x,y) = p_B = 0.285$  and  $0.40$

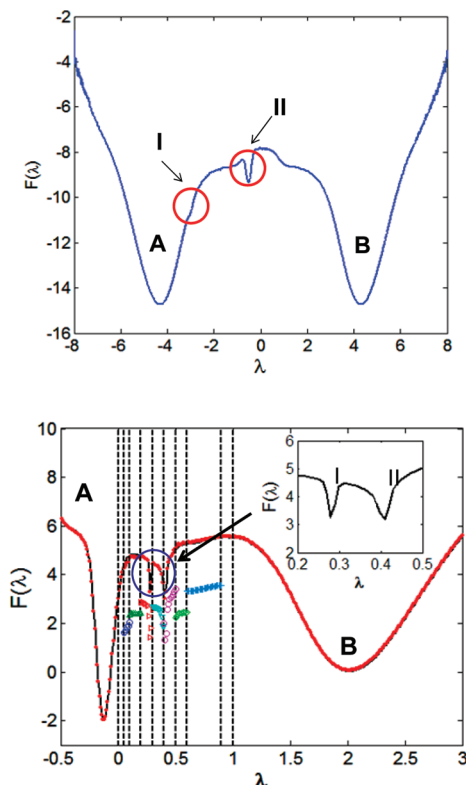


**Figure 11.** Free energy  $F$  for the 2D potential energy surface no. 2. (a, top)  $F$  profile along the  $x$  coordinate as reaction coordinate. (b, bottom) Sequence of measured free energies  $F(\lambda)$  along optimized reaction coordinate model ( $\lambda = p_B$ ) from the FFS-US simulations. The  $\lambda$  windows are demarcated by dotted lines and the partial  $F(\lambda)$  curves in those windows are stitched up into a continuous  $F(\lambda)$  function (red dot).  $F(\lambda)$  in the initial region A and final region B was obtained via standard US simulations.  $F(\lambda)$  from a standard brute force simulation is also shown (solid black line).

**TABLE 5: Data for the FFS-US Simulations with the Energy Potential Surface No. 2 and Seven Windows  $w_i$  between States A and B<sup>a</sup>**

$w_i$ [ $\lambda_{i-1}, \lambda_{i+1}$ ]	$\lambda_i$	$\lambda_{i+1}$	$N_{\text{win}}^{(i)} [\Delta t]$	% $R_{\text{FFS}}$
1	0.05	0.10	$2.5 \times 10^5$	38
2	0.10	0.20	$9.8 \times 10^5$	38
3	0.20	0.30	$9.8 \times 10^5$	39
4	0.30	0.40	$9.8 \times 10^5$	52
5	0.40	0.50	$9.8 \times 10^5$	83
6	0.50	0.60	$9.8 \times 10^5$	95
7	0.60	0.90	$8.9 \times 10^6$	89

<sup>a</sup>  $N_{\text{bin}} = 5 \times 10^3$ .

for intermediates states I and II, respectively. In obtaining the  $p(\lambda)$  distribution, FFS-US capitalizes on the  $h_i^{\text{FFS}}(\lambda)$  data which contributed between 38% to 95% in terms of %  $R_{\text{FFS}}$  (see Table 5).

The optimized reaction coordinate model shows that particles visiting the intermediate state II have greater probability to commit to region B compared to particles visiting state I. Consequently, the rate constant for the paths passing through II (i.e.,  $A \rightarrow \text{II} \rightarrow \text{B}$  and  $A \rightarrow * \rightarrow \text{II} \rightarrow \text{B}$ ) is expected to be higher than those for transitions passing through I (i.e.,  $A \rightarrow \text{I} \rightarrow \text{B}$  and  $A \rightarrow * \rightarrow \text{I} \rightarrow \text{B}$ ); see section III E for the notation details. Consistent with the density map ( $P_{\text{TSE}}$ ) in Figure 10b, the TPE should contain more pathways connecting the stable states through state II than through state I. Figure 12a shows a schematic illustration for all the possible transitions connecting stable states A and B. The rate constant estimates for transition

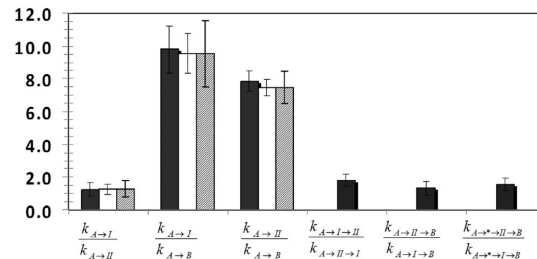
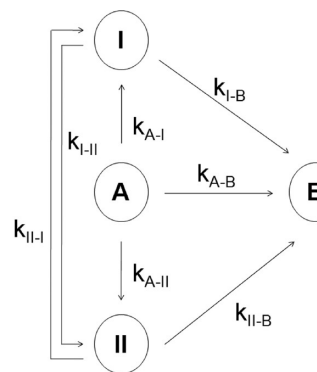


**Figure 12.** (a, top) Schematic illustration of the reactions involved in the A to B transition for the 2D potential energy surface no. 2.<sup>13</sup> (b, bottom) Ratio of the multiple state probabilities (i.e.,  $k_A/k_A^*$ ) for different transitions between the four basins: from a single multiple state FFS simulation (black bars), independent FFS simulations (white bars) and from Figure 3 of ref 13 (patterned bars). From a single FFS simulation connecting stable states A and B, rate constant values can be estimated for the transitions  $k_{A \rightarrow B}$ ,  $k_{A \rightarrow I \rightarrow B}$ ,  $k_{A \rightarrow II \rightarrow B}$ ,  $k_{A \rightarrow * \rightarrow I \rightarrow B}$ ,  $k_{A \rightarrow * \rightarrow II \rightarrow B}$ ,  $k_{A \rightarrow I}$ ,  $k_{A \rightarrow II}$ ,  $k_{A \rightarrow I \rightarrow II}$ ,  $k_{A \rightarrow II \rightarrow I}$ , and  $k_{A \rightarrow * \rightarrow I \rightarrow B}$ .

from state A to B and passing through  $M$  metastable states  $\mathbf{m}$  and from state A to a particular  $m$  state were estimated by eqs 18 and 20, respectively. The results in Figure 12b for the ratio of the multiple transition rate constants show good agreement with the results presented in Figure 3 of ref 13 and those we obtained (as a further test) from independent FFS simulations targeting a particular transition. The rate constants for transitions from  $A \rightarrow I$  and  $A \rightarrow II$  are similar in magnitude whereas the rate constant  $A \rightarrow B$  ( $k_{A \rightarrow B}$ ) for trajectories connecting A and B without passing through an intermediate state is a factor of  $\sim 7$  lower. Furthermore, transitions to the intermediate state II through state I ( $A \rightarrow I \rightarrow II$ ) are a factor of  $\sim 2$  larger than those passing first through state II before committing to state I ( $A \rightarrow II \rightarrow I$ ). Hence, as expected from the  $p_B$  surface, once the system committed to the intermediate state II, it is most likely to make a transition to the basin of attraction B. The rate for transitions through intermediate state II ( $A \rightarrow * \rightarrow II \rightarrow B$ ) are a factor of  $\sim 1.5$  larger than those through state I ( $A \rightarrow * \rightarrow I \rightarrow B$ ) and a factor 3.3 larger than those that go directly from A to B ( $A \rightarrow B$ ), indicating that most paths arriving to B come from state II. Moreover, transitions through intermediate state II only ( $A \rightarrow II \rightarrow B$ ) are a factor of  $\sim 1.3$  larger than those through state I only ( $A \rightarrow I \rightarrow B$ ). The rates for the  $A \rightarrow II \rightarrow B$  and  $A \rightarrow I \rightarrow B$  transitions are 63 and 74% of those for the  $A \rightarrow * \rightarrow II \rightarrow B$  and  $A \rightarrow * \rightarrow I \rightarrow B$  transitions, respectively, indicating that the amount of  $I \leftrightarrow II$  transitions is significant.

#### IV. Conclusions

This paper complements two previous articles<sup>11,12</sup> in which we presented several optimization algorithms for FFS-type simulations. The new algorithm (FFS-US) uses the FFS setup to obtain the equilibrium probability distribution once the

kinetics of the system was simulated via FFS. The scheme is straightforward to implement and does not involve the use of biasing weights. The correct probability distribution is computed by combining histogram data from both the transition path ensemble obtained from FFS and an extra US performed for several partial paths. By design, the computational effort is set to be the same as that of a standard US simulation so as to have comparable statistical errors in the free energy data. Our proof of principle applications demonstrate the validity of the FFS-US for computing the equilibrium distribution of systems involving free-energy barriers having multiple local minima.

In FFS-US, the FFS runs typically provided more than half of the total statistical data needed to evaluate the probability distributions, with US providing the balance. Perhaps more importantly, the initial interfacial points provided by FFS are ideal for the subsequent US because they are obtained along an optimized order parameter (which should help minimize hysteretic effects) with windows positioned for computational efficiency. In this manner, the resulting free energy is mapped along a most useful coordinate while concentrating the US in the more difficult/important regions. Also, FFS-US should be helpful in reducing window kinetic trapping which tends to occur with conventional window-based US methods: by sampling windows using several paths initiated at different configurations (inherited from FFS) of a given interface, the system is allowed to more broadly explore the phase space around the barriers.

We also extended the original FFS formalism so that sampling of pathways passing through multiple intermediate states can be monitored to allow the estimation of rate constants of all possible forward transitions connecting stable states A and B through intermediates states and from A to any intermediate state. We envision that this method will be a valuable tool to study complex systems where the transition between the two main basin is mediated by partial transitions through distinct metastable states.

**Acknowledgment.** The authors are grateful for support from the National Science Foundation Award 0553719.

## References and Notes

- (1) Allen, R. J.; Frenkel, D.; ten Wolde, P. R. *J. Chem. Phys.* **2006**, *124*, 024102.
- (2) Allen, R. J.; Warren, P. B.; ten Wolde, P. R. *Phys. Rev. Lett.* **2005**, *94*, 018104.
- (3) Frenkel, D.; Smit, B. *Understanding Molecular Simulation: From Algorithms to Applications*, 2nd ed.; Academic: Boston, MA, 2002.
- (4) Radhakrishnan, R.; Schlick, T. *J. Chem. Phys.* **2004**, *121*, 2436–2444.
- (5) Moroni, D.; van Erp, T. S.; Bolhuis, P. G. *Phys. Rev. E* **2005**, *71*.
- (6) Faradjian, A. K.; Elber, R. *J. Chem. Phys.* **2004**, *120*, 10880–10889.
- (7) Ytreberg, F. M.; Zuckerman, D. M. *Proc. Natl. Acad. Sci. U.S.A.* **2008**, *105*, 7982–7987.
- (8) Valeriani, C.; Allen, R. J.; Morelli, M. J.; Frenkel, D.; ten Wolde, P. R. *J. Chem. Phys.* **2007**, *127*, 114109–11.
- (9) Bolhuis, P. G. *J. Chem. Phys.* **2008**, *129*, 114108–13.
- (10) Warmflash, A.; Bhimalapuram, P.; Dinner, A. R. *J. Chem. Phys.* **2007**, *127*, 154112–8.
- (11) Borrero, E. E.; Escobedo, F. A. *J. Chem. Phys.* **2007**, *127*, 164101–17.
- (12) Borrero, E. E.; Escobedo, F. A. *J. Chem. Phys.* **2008**, *129*, 024115–16.
- (13) Rogal, J.; Bolhuis, P. G. *J. Chem. Phys.* **2008**, *129*, 224107–9.
- (14) Allen, R. J.; Frenkel, D.; ten Wolde, P. R. *J. Chem. Phys.* **2006**, *124*, 194111.
- (15) Moroni, D.; van Erp, T. S.; Bolhuis, P. G. *Physica A (Amsterdam)* **2004**, *340*, 395–401.
- (16) Virnau, P.; Muller, M. *J. Chem. Phys.* **2004**, *120*, 10925–10930.
- (17) Ferrenberg, A. M.; Swendsen, R. H. *Phys. Rev. Lett.* **1989**, *63*, 1195–1198.
- (18) Escobedo, F. A.; Abreu, C. R. A. *J. Chem. Phys.* **2006**, *124*.
- (19) Abkevich, V. I.; Gutin, A. M.; Shakhnovich, E. I. *Fold Des.* **1996**, *13*, 221–230.
- (20) Borrero, E. E.; Escobedo, F. A. *J. Chem. Phys.* **2006**, *125*, 164904–14.
- (21) Chopra, M.; Malshe, R.; Reddy, A. S.; de Pablo, J. J. *J. Chem. Phys.* **2008**, *128*, 114104–5.
- (22) Ma, A.; Dinner, A. R. *J. Phys. Chem. B* **2005**, *109*, 6769–6779.
- (23) Peters, B.; Trout, B. L. *J. Chem. Phys.* **2006**, *125*, 054108–10.

JP809103K